Supplementary Information for:

Shear-induced liquid-crystalline phase transition behavior of colloidal solutions of hydroxyapatite nanorod composites

Satoshi Kajiyama,[a] Hiroki Iwase,[b] Masanari Nakayama,[a] Rino Ichikawa,[a] Daisuke Yamaguchi,[a] Hideki Seto,*[,c] Takashi Kato*[,a]

[a]Department of Chemistry and Biotechnology, School of Engineering, The University of Tokyo, 7-3-1 Hongo, Bunkyo-ku, Tokyo 113-8656, Japan

[b]Neutron Science and Technology Center, Comprehensive Research Organization for Science and Society (CROSS), 162-1 Shirataka, Tokai, Ibaraki 319-1106, Japan

[c]J-PARC Center, High Energy Accelerator Research Organization, 203-1 Shirataka, Tokai, Ibaraki 319-1106, Japan.

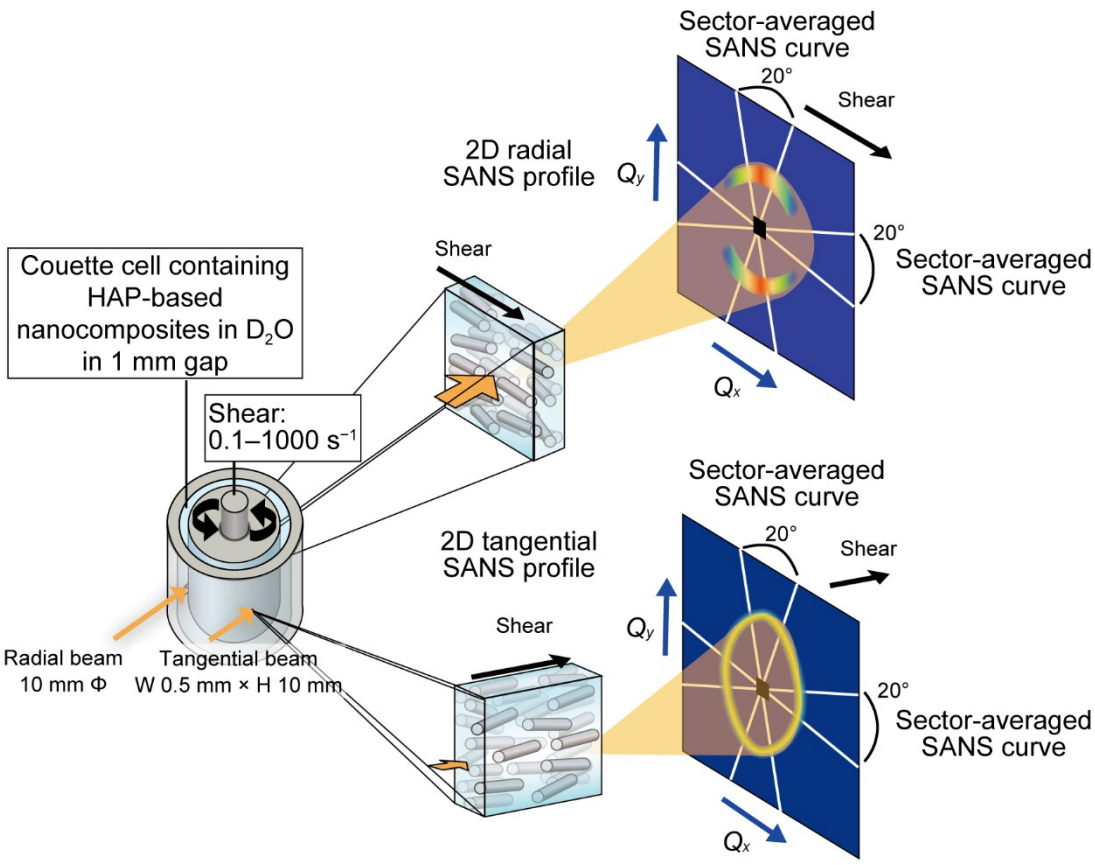

Fig. S1 Schematic illustration for Rheo-SANS measurement of colloidal solutions of HAP-based nanocomposites.

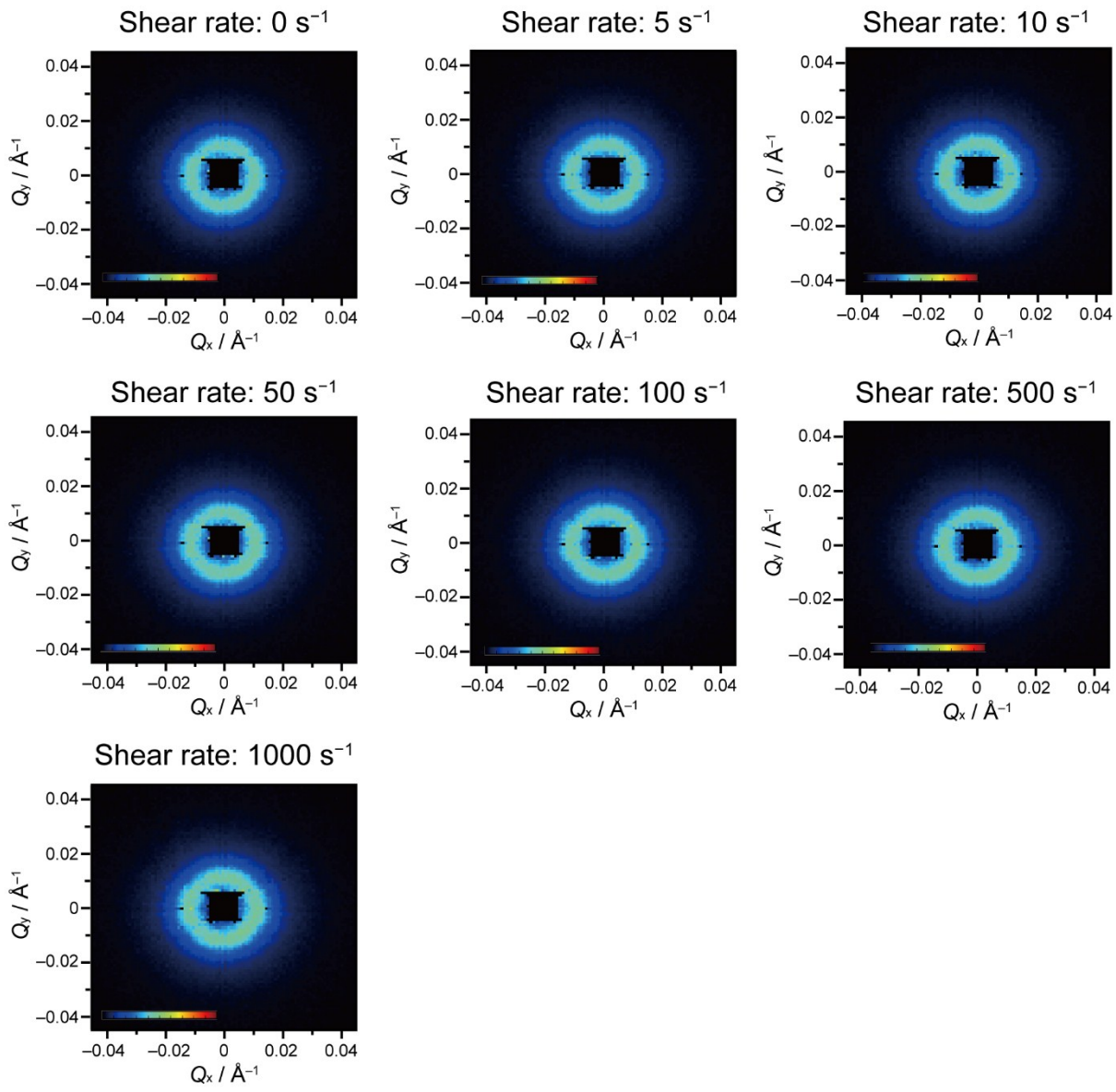

Fig. S2 2D radial SANS profiles of a colloidal solution of HAP-based nanocomposites at 3.3 vol% with various shear rates.

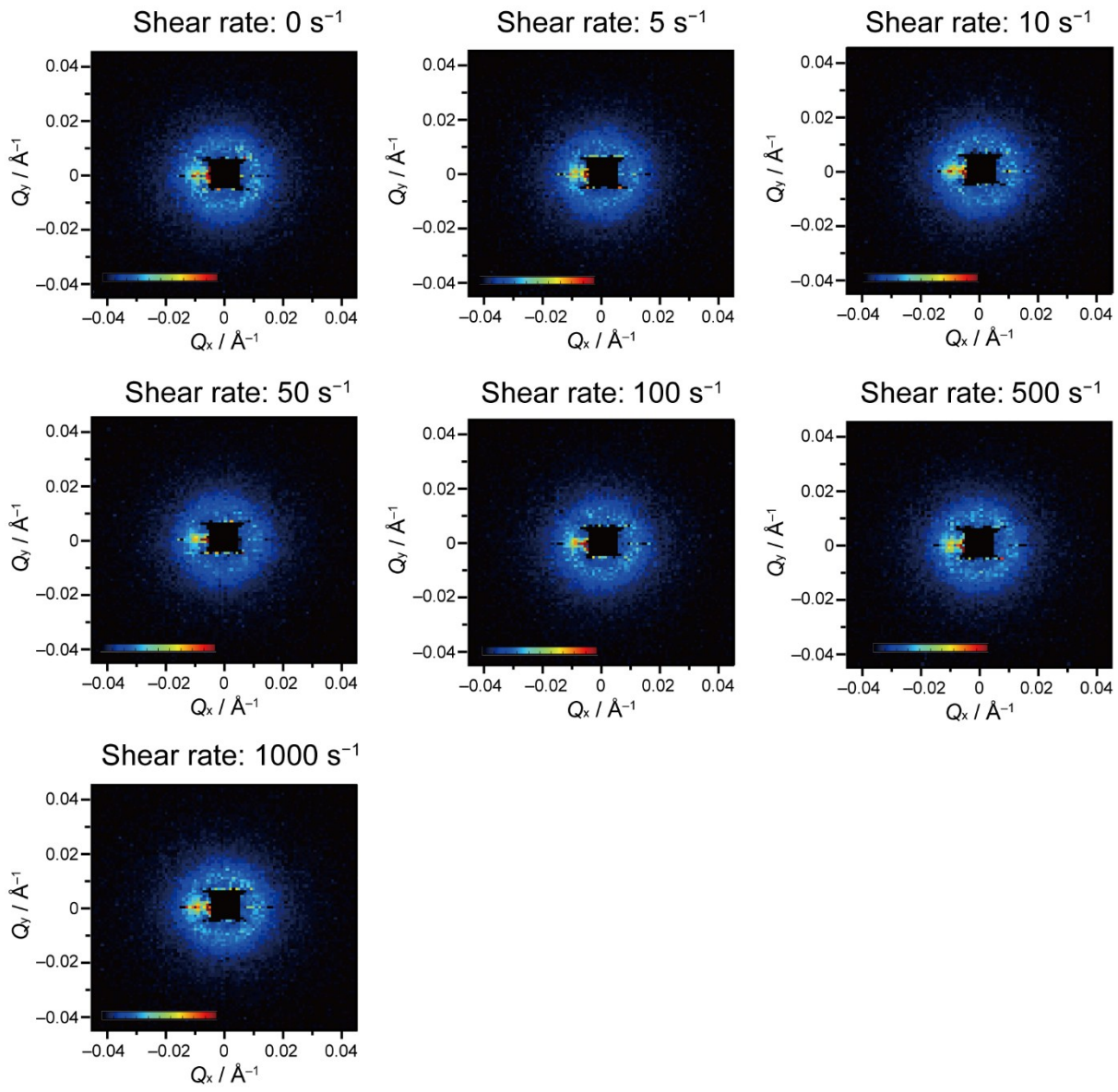

Fig. S3 2D tangential SANS profiles of a colloidal solution of HAP-based nanocomposites at 3.3 vol% with various shear rates.

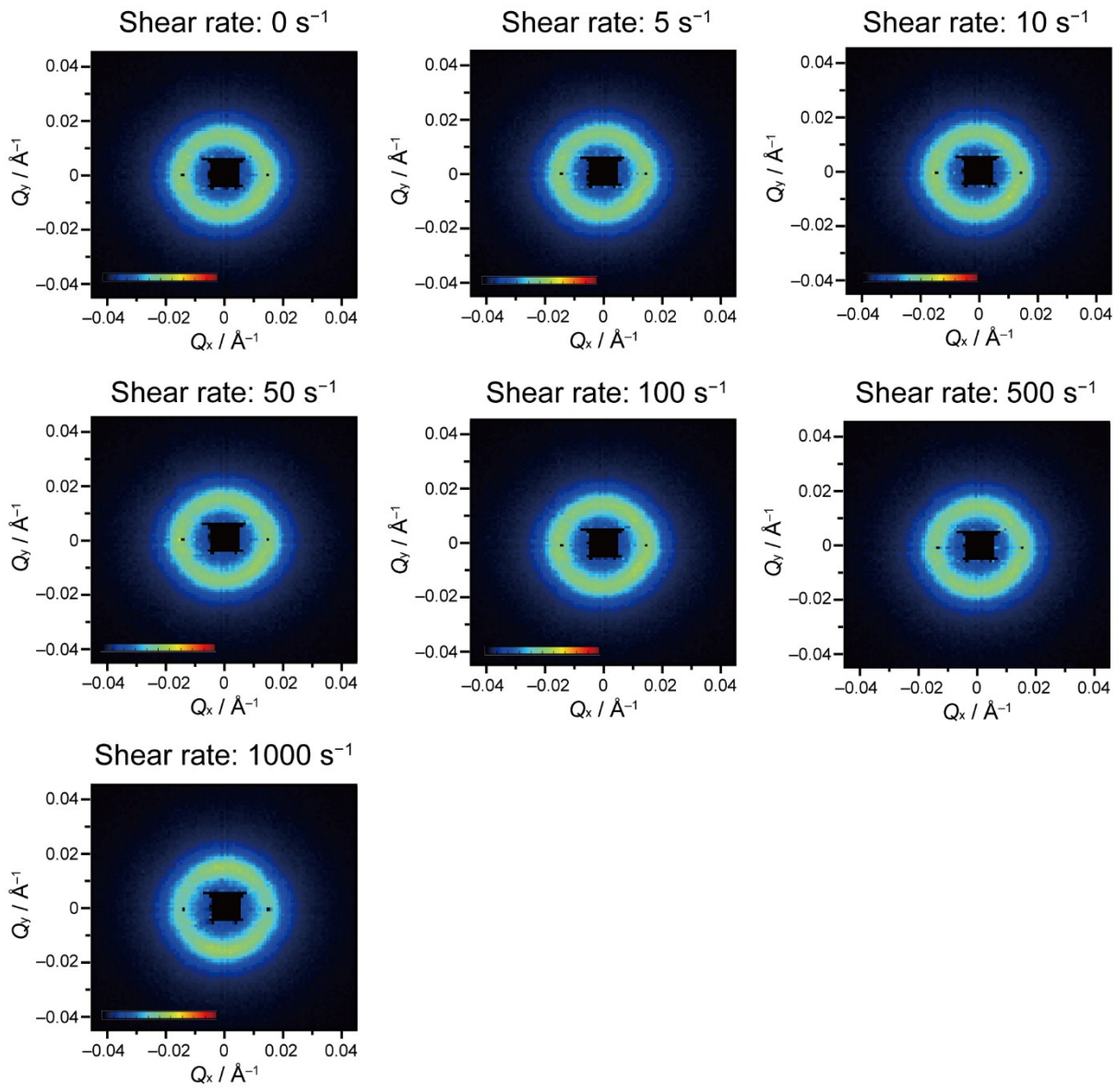

Fig. S4 2D radial SANS profiles of a colloidal solution of HAP-based nanocomposites at 4.4 vol% with various shear rates.

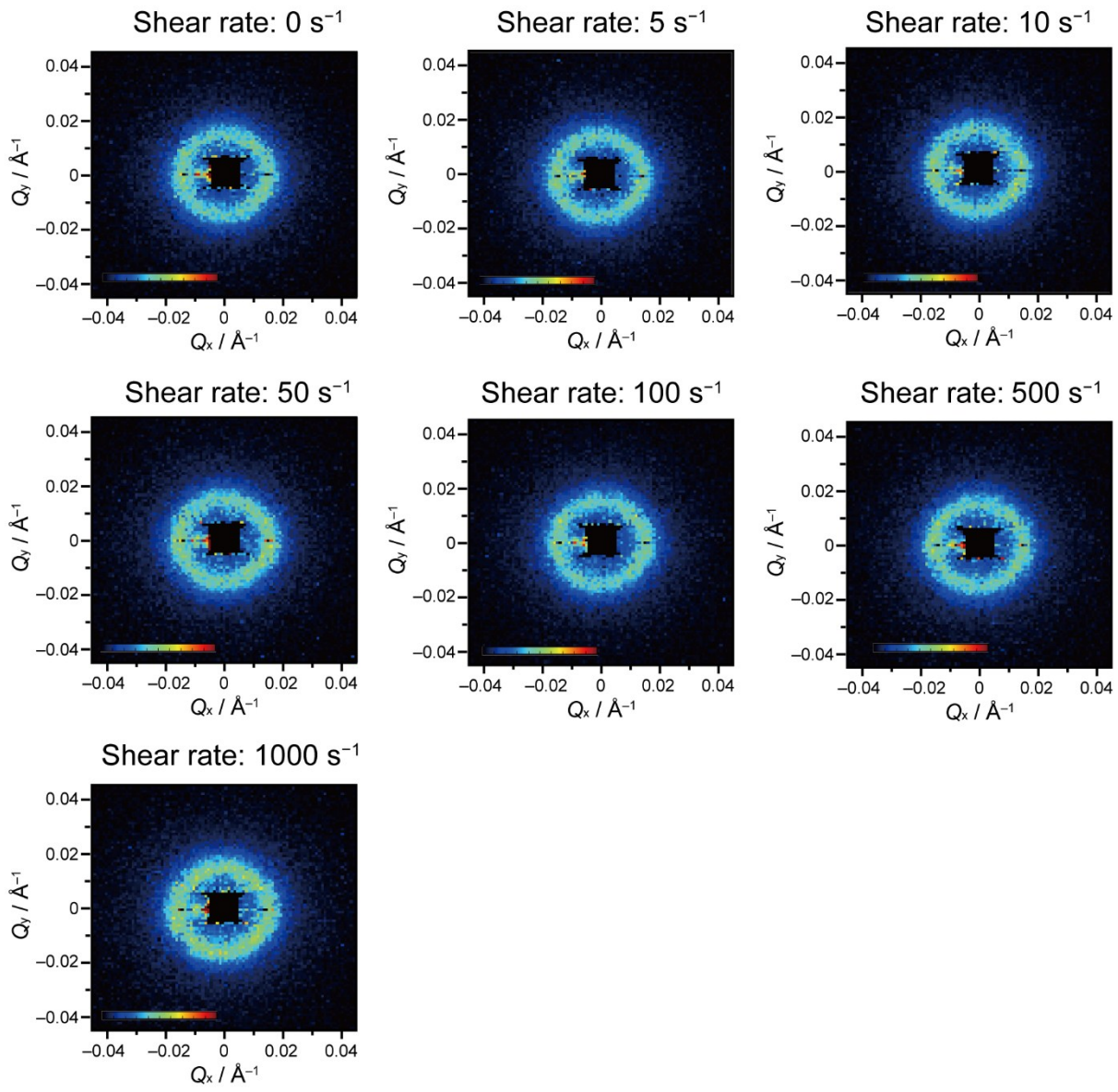

Fig. S5 2D tangential SANS profiles of a colloidal solution of HAP-based nanocomposites at 4.4 vol% with various shear rates.

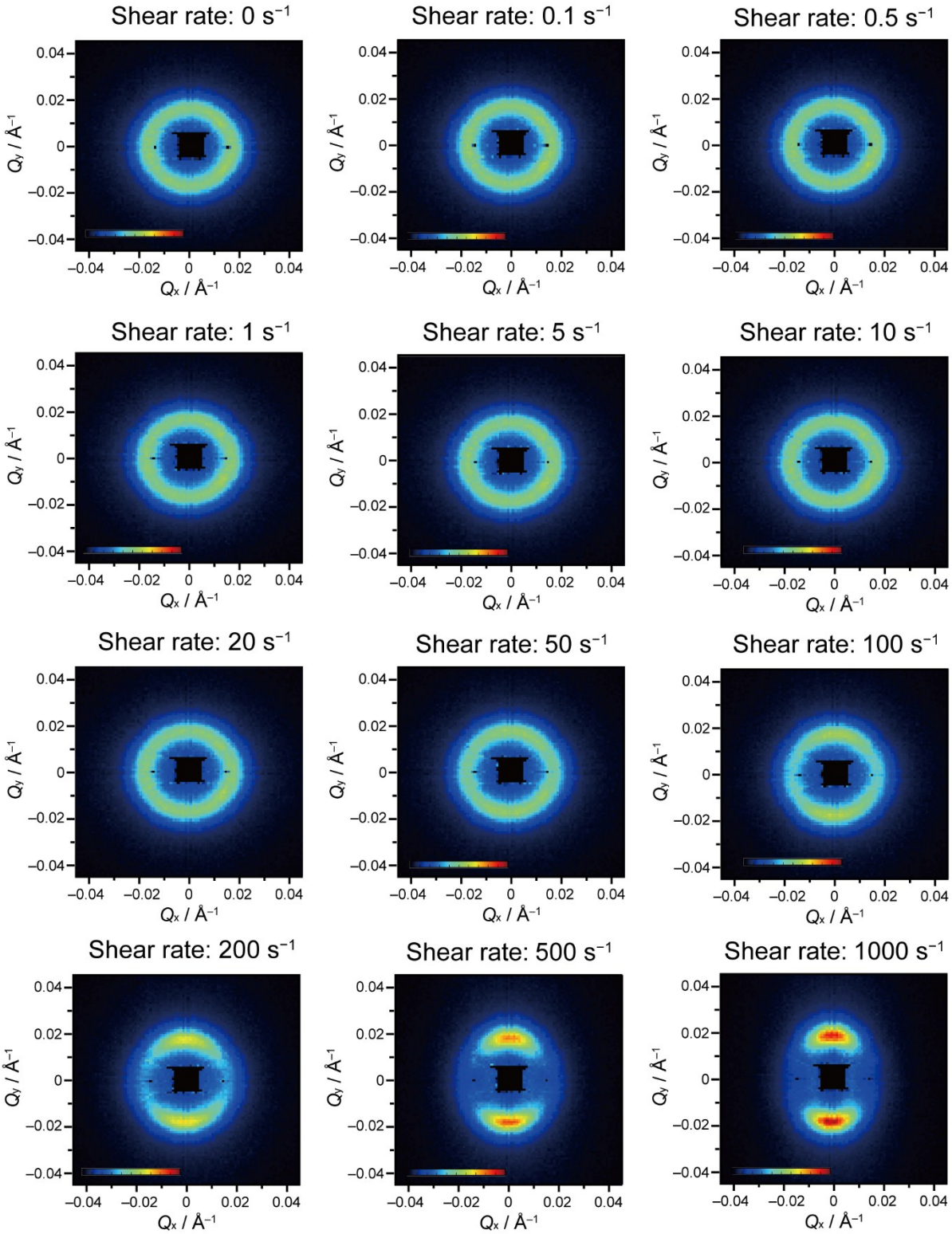

Fig. S6 2D radial SANS profiles of a colloidal solution of HAP-based nanocomposites at 6.7 vol% with various shear rates.

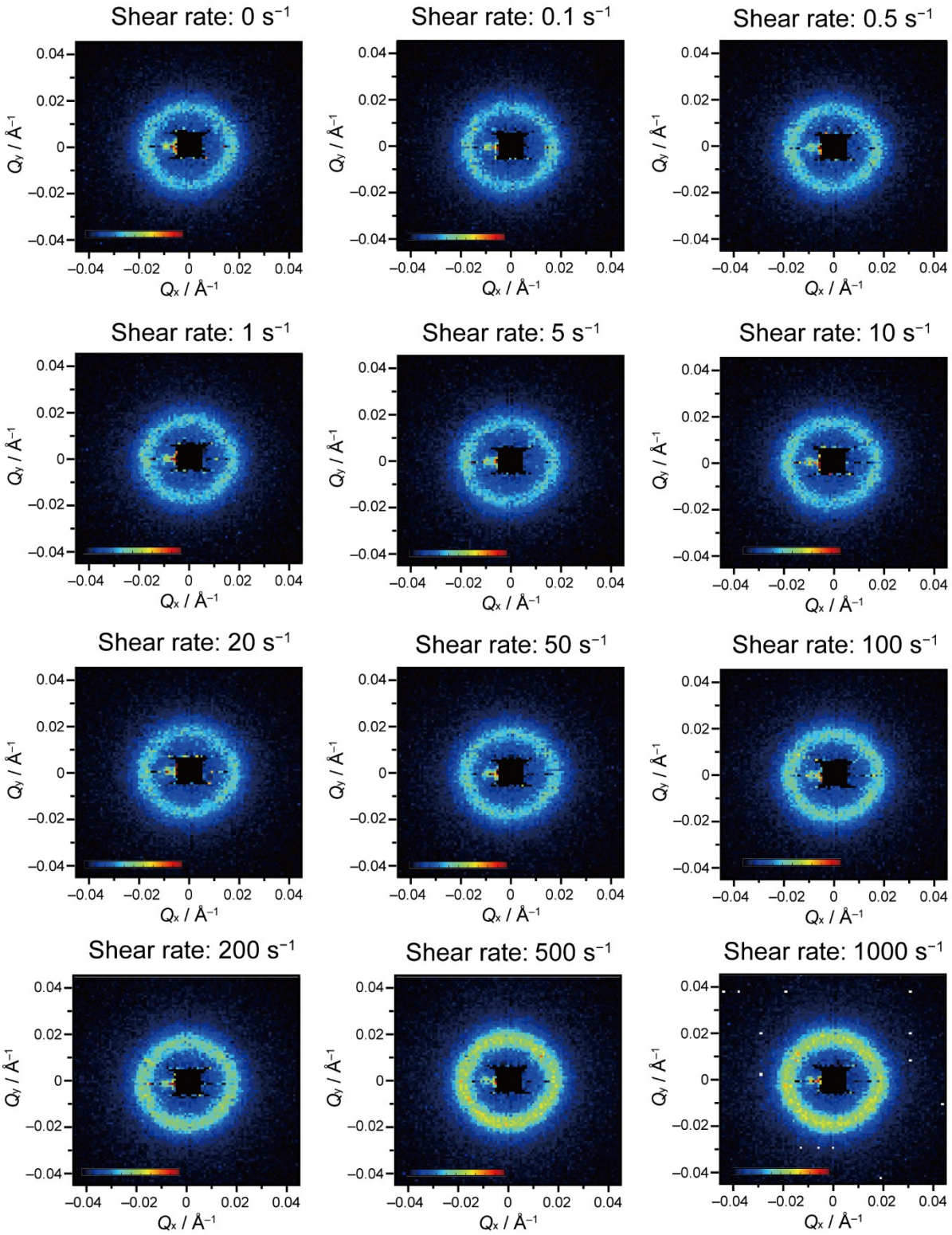

Fig. S7 2D tangential SANS profiles of a colloidal solution of HAP-based nanocomposites at 6.7 vol% with various shear rates.

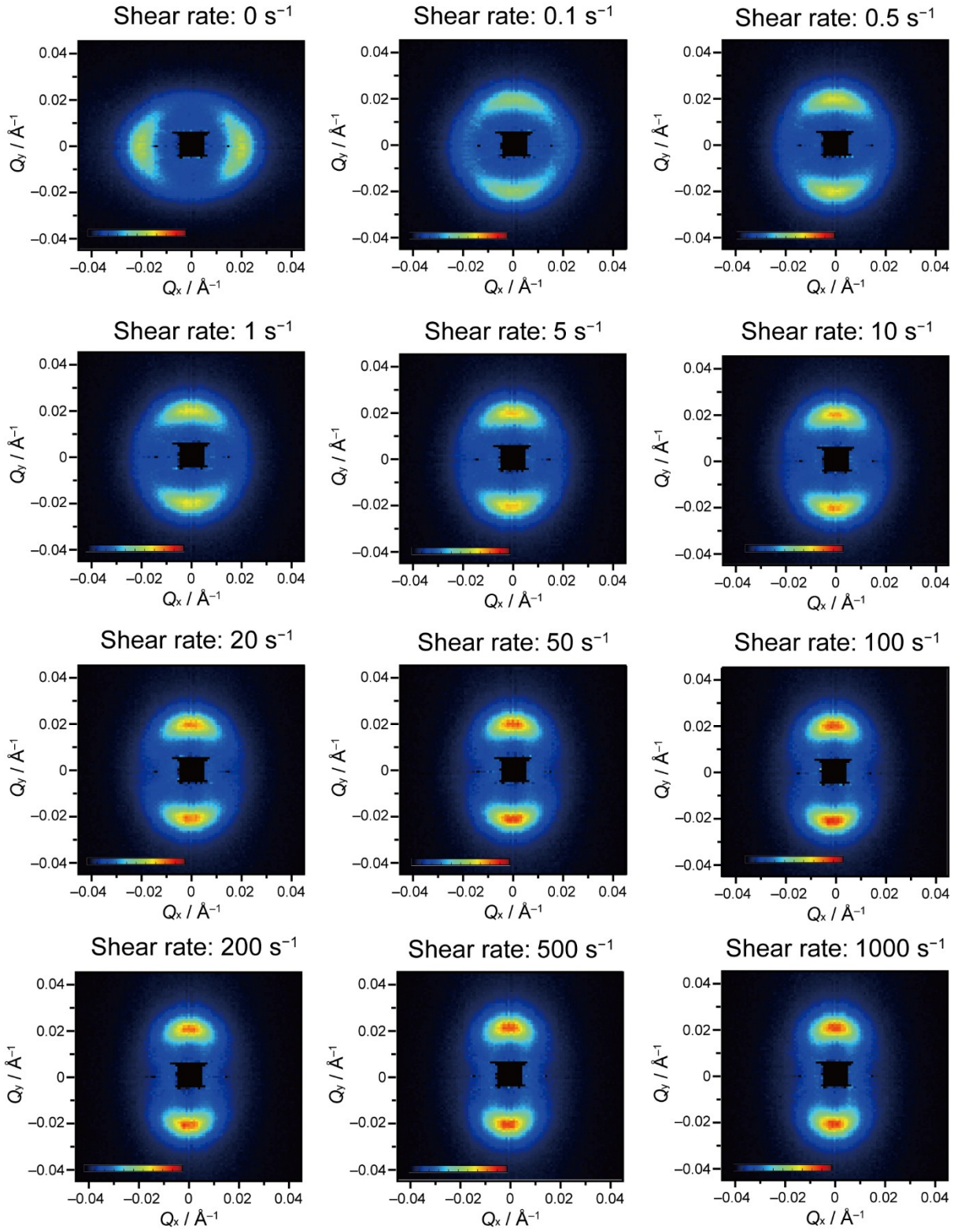

Fig. S8 2D radial SANS profiles of a colloidal solution of HAP-based nanocomposites at 8.7 vol% with various shear rates.

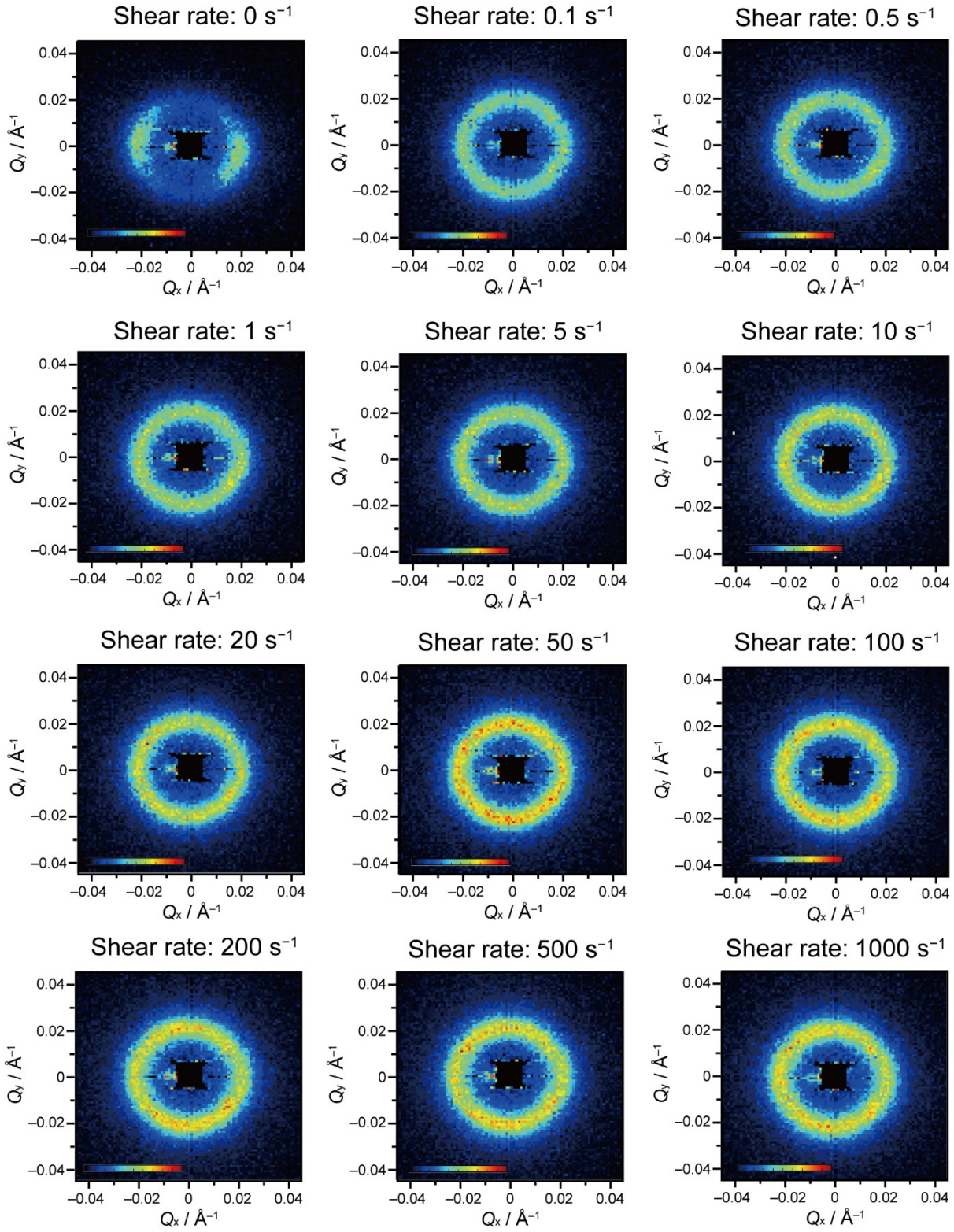

Fig. S9 2D tangential SANS profiles of a colloidal solution of HAP-based nanocomposites at 8.7 vol% with various shear rates.

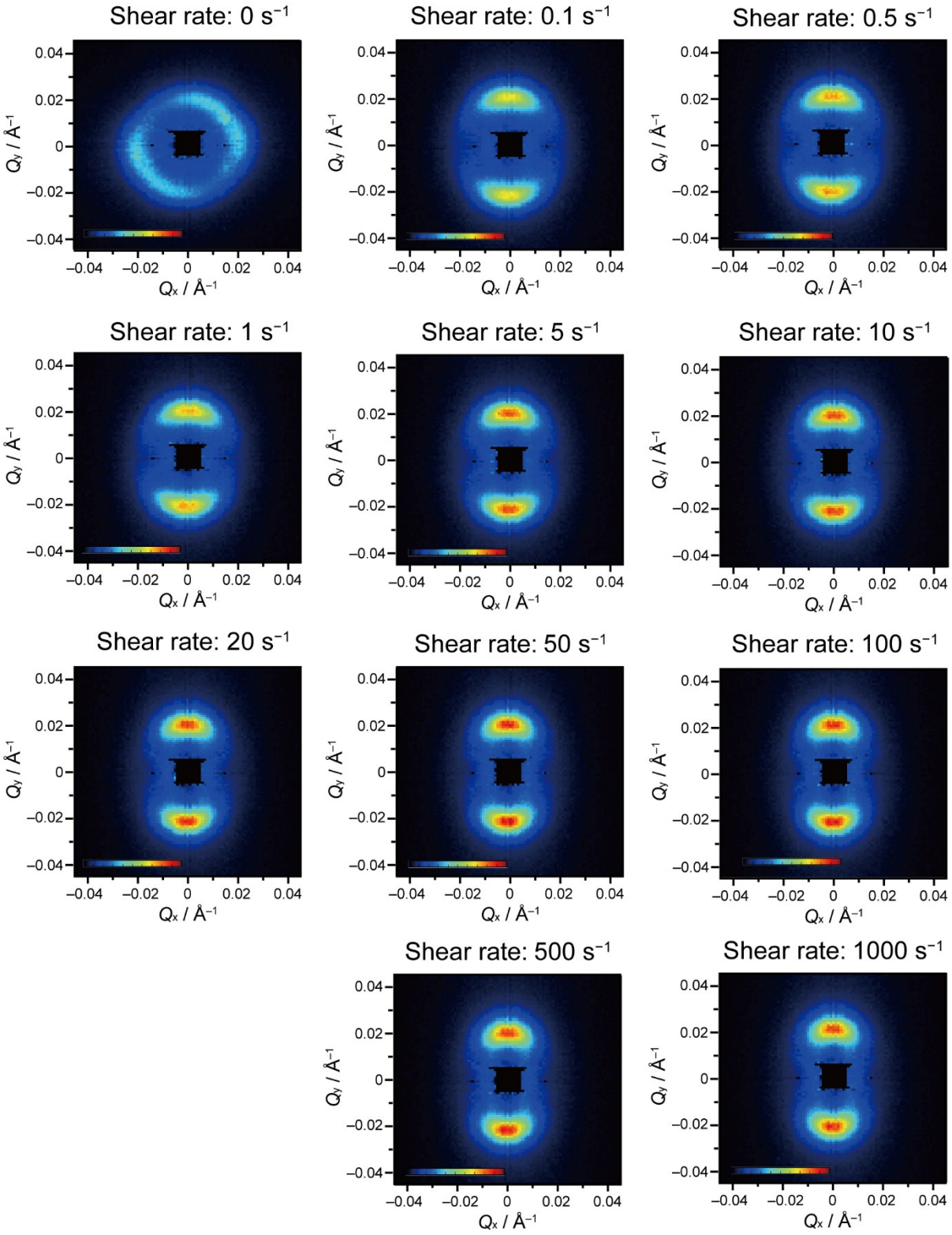

Fig. S10 2D radial SANS profiles of a colloidal solution of HAP-based nanocomposites at 9.7 vol% with various shear rates.

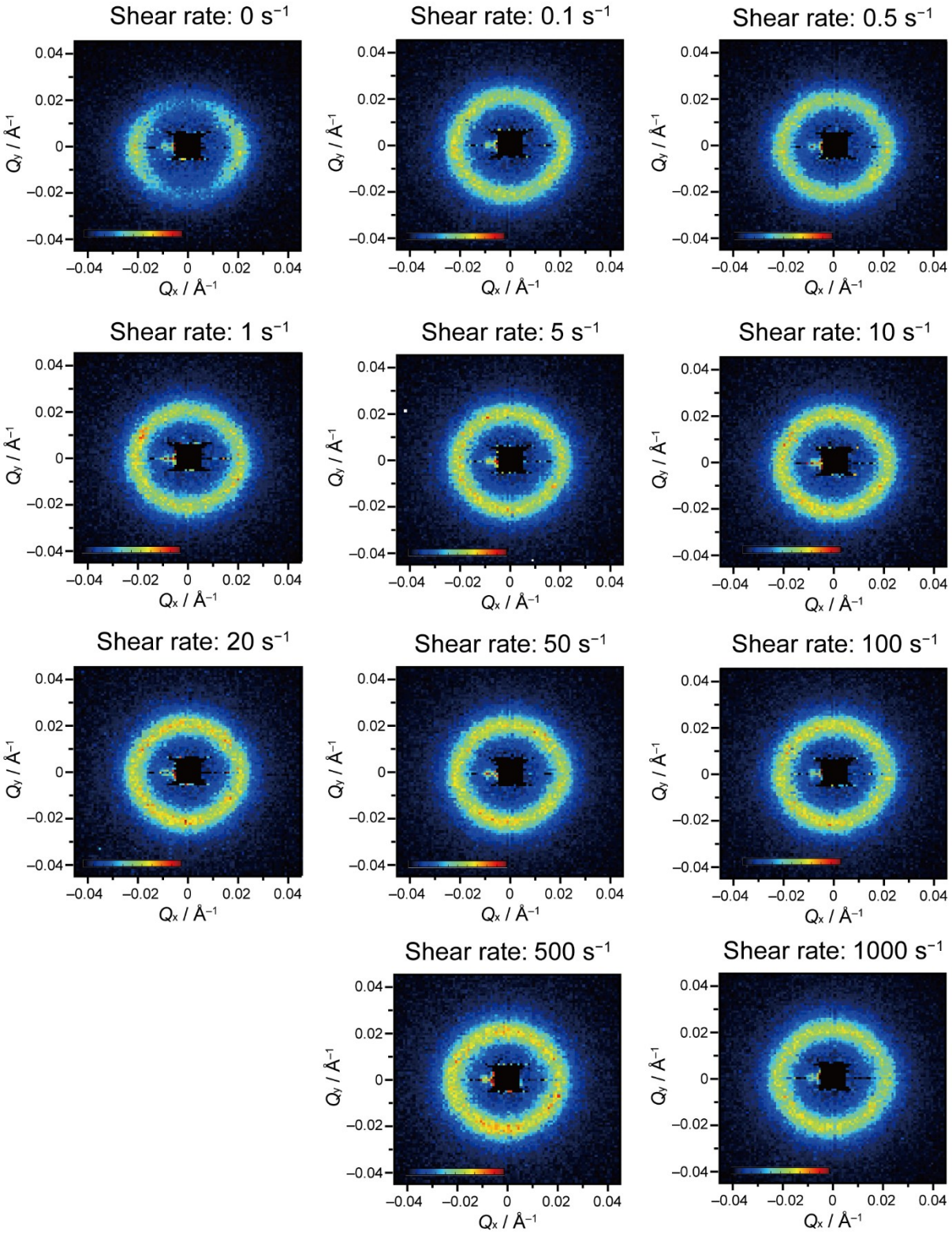

Fig. S11 2D tangential SANS profiles of a colloidal solution of HAP-based nanocomposites at 9.7 vol% with various shear rates.

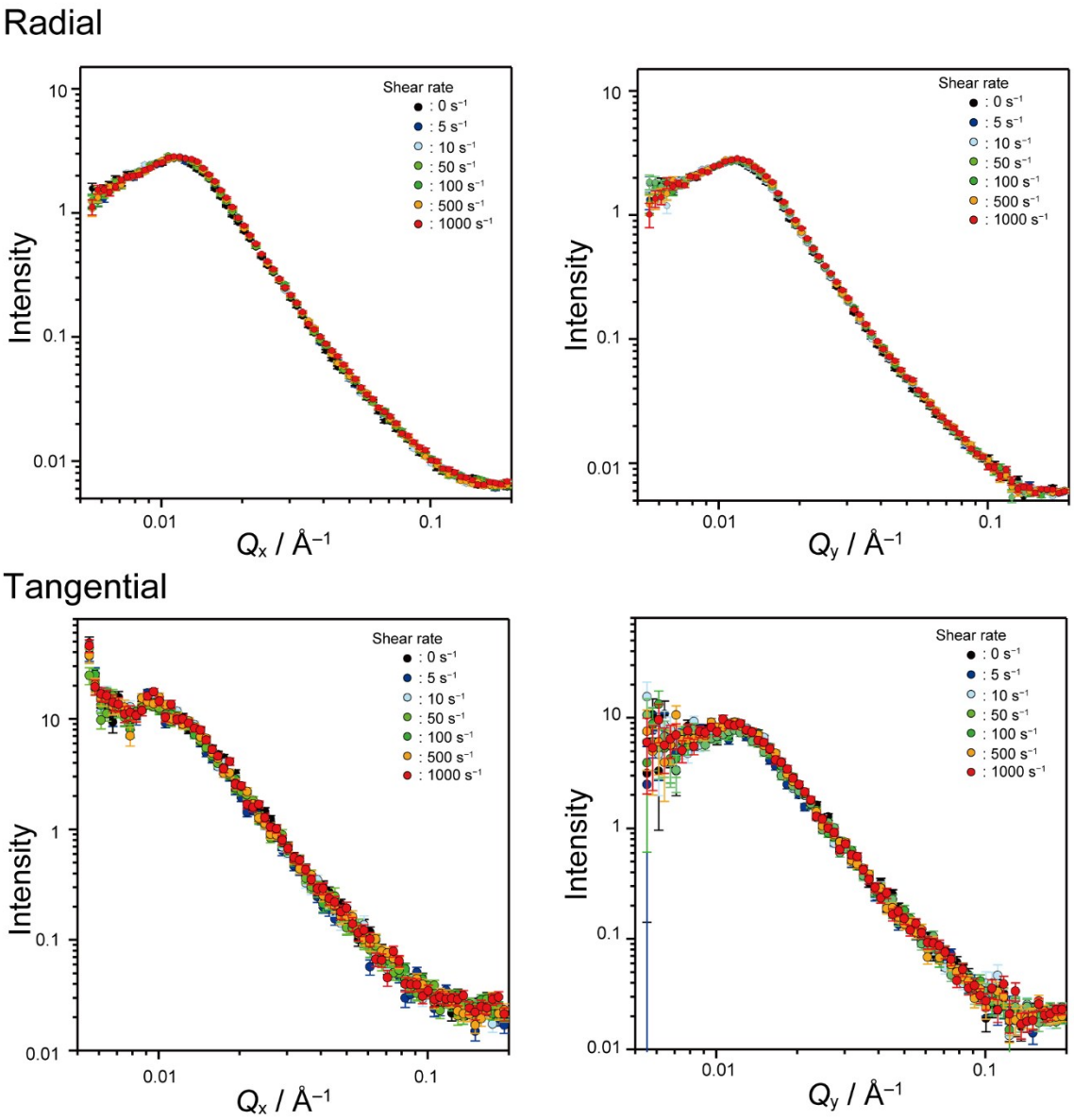

Fig. S12 Sector-averaged SANS curves for a colloidal solution of HAP-based nanocomposites at 3.3 vol% under various shear rates with an azimuthal angle of ± 10°.

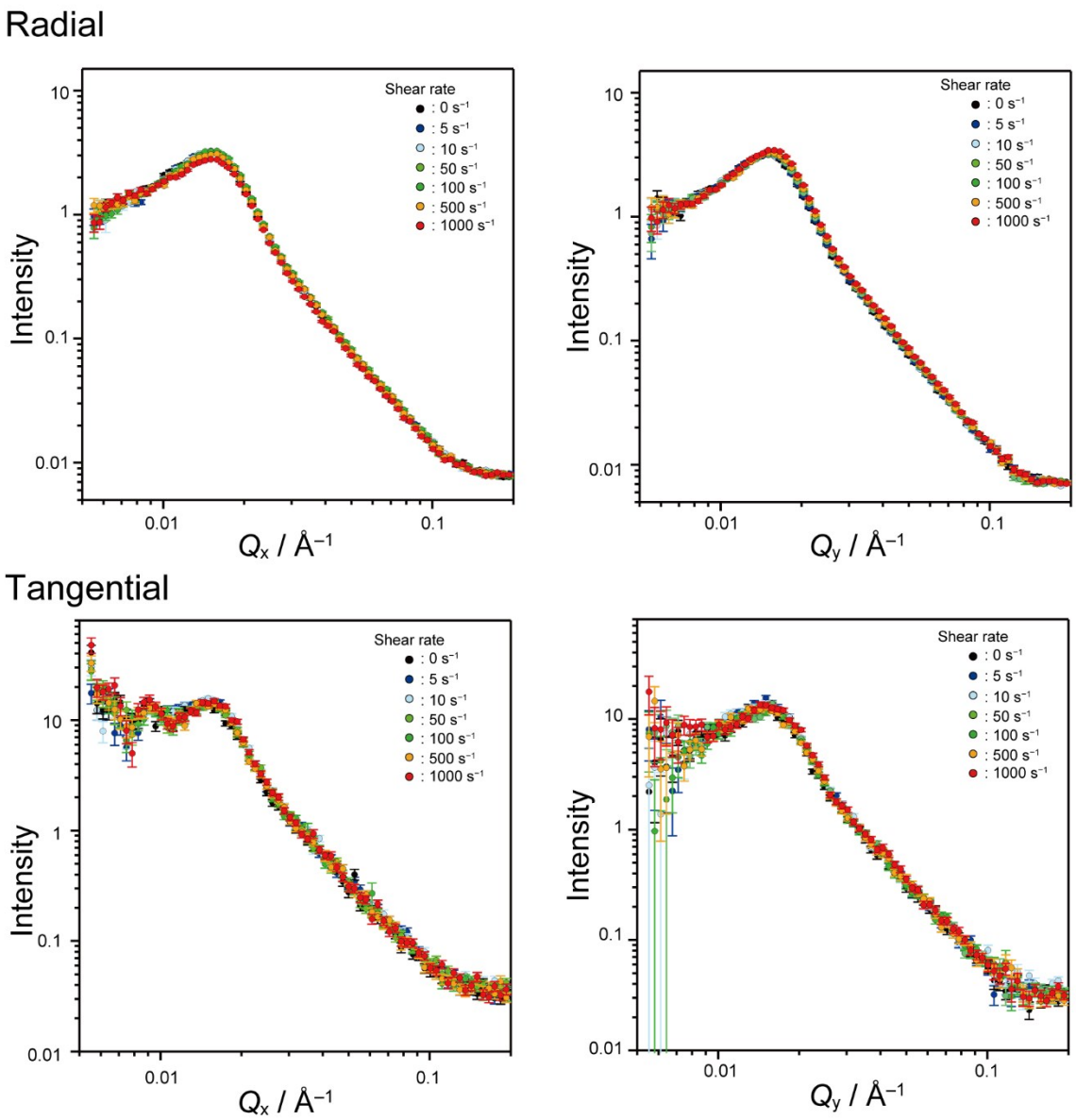

Fig. S13 Sector-averaged SANS curves for a colloidal solution of HAP-based nanocomposites at 4.4 vol% under various shear rates with an azimuthal angle of ± 10°.

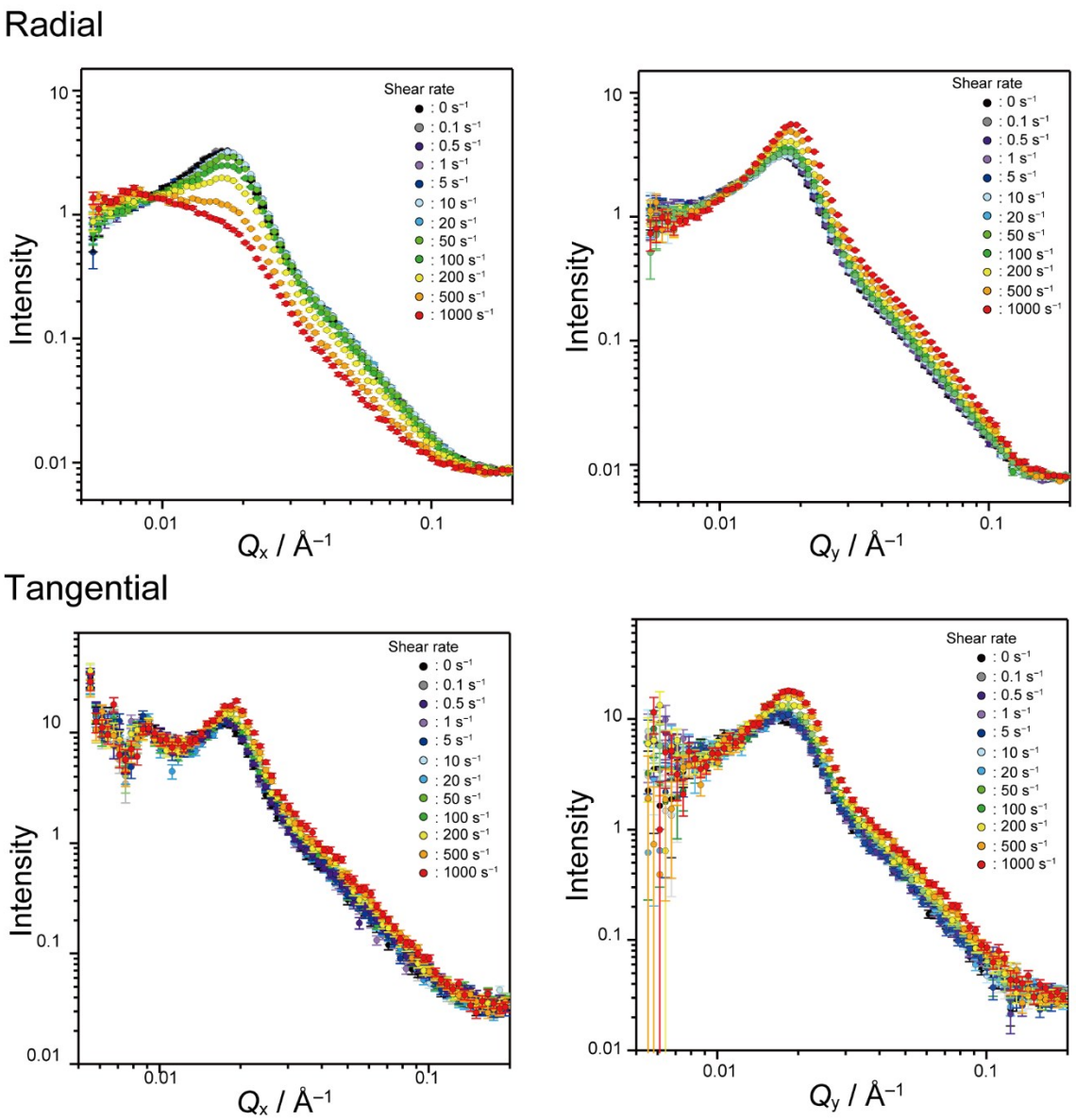

Fig. S14 Sector-averaged SANS curves for a colloidal solution of HAP-based nanocomposites at 6.7 vol% under various shear rates with an azimuthal angle of ± 10°.

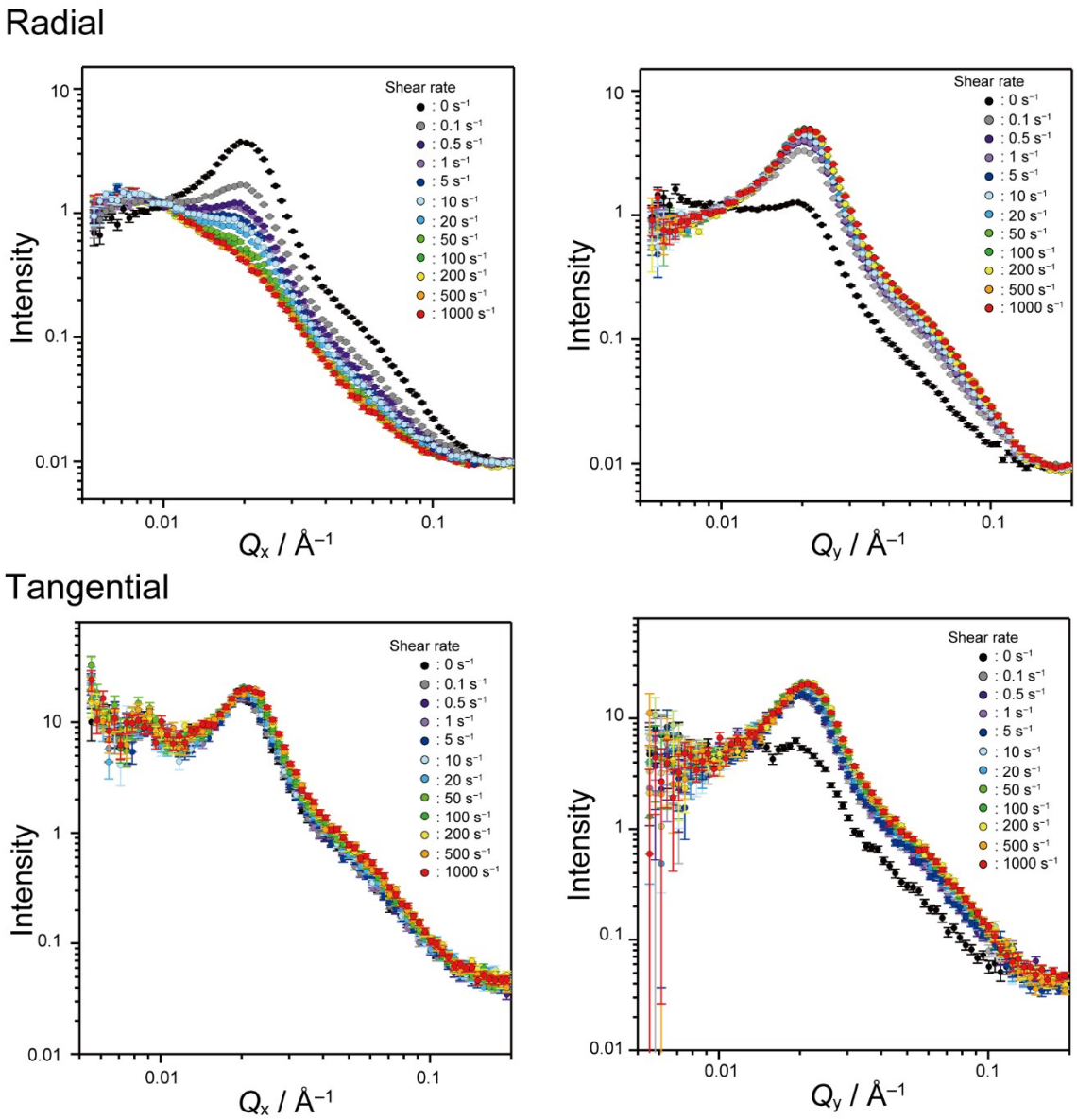

Fig. S15 Sector-averaged SANS curves for a colloidal solution of HAP-based nanocomposites at 8.7 vol% under various shear rates with an azimuthal angle of ± 10°.

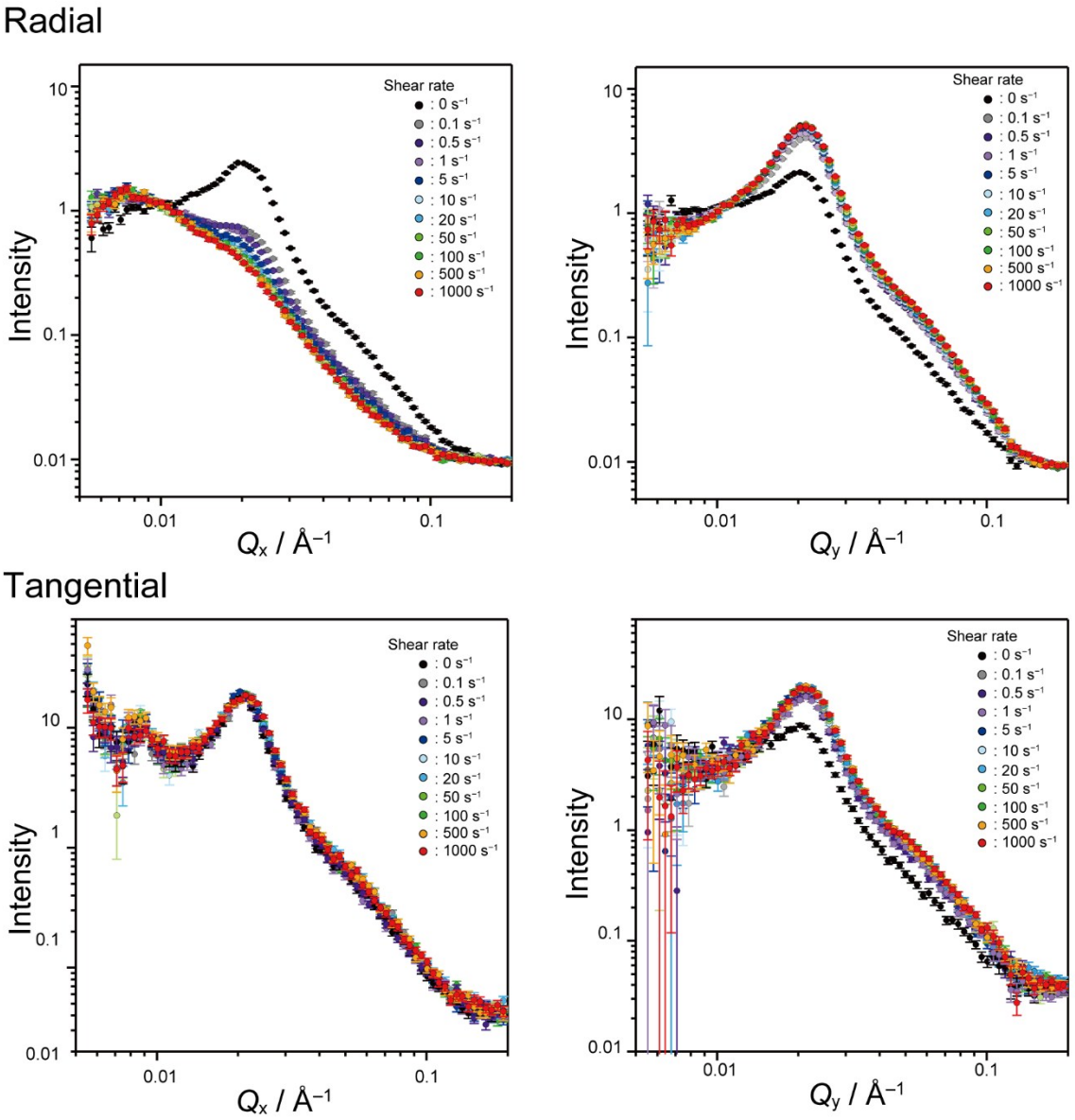

Fig. S16 Sector-averaged SANS curves for a colloidal solution of HAP-based nanocomposites at 9.7 vol% under various shear rates with an azimuthal angle of ± 10°.

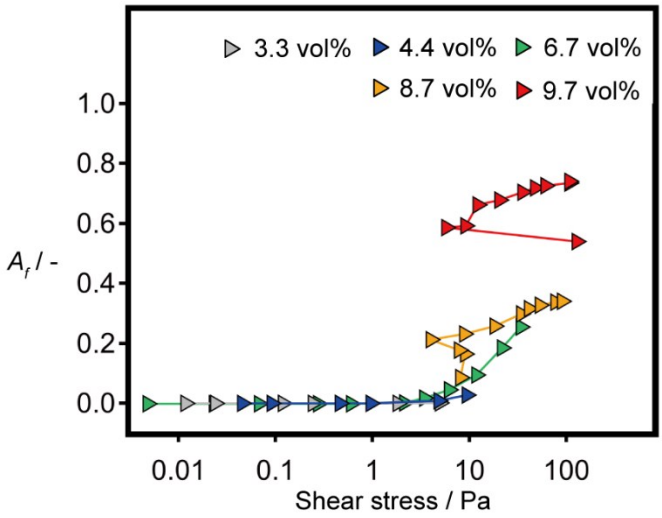

Fig. S17 Plots of Alignment degree vs shear stress of colloidal solutions of HAP-based nanocomposites with various concentrations, showing the required shear stress for the alignment treatment.

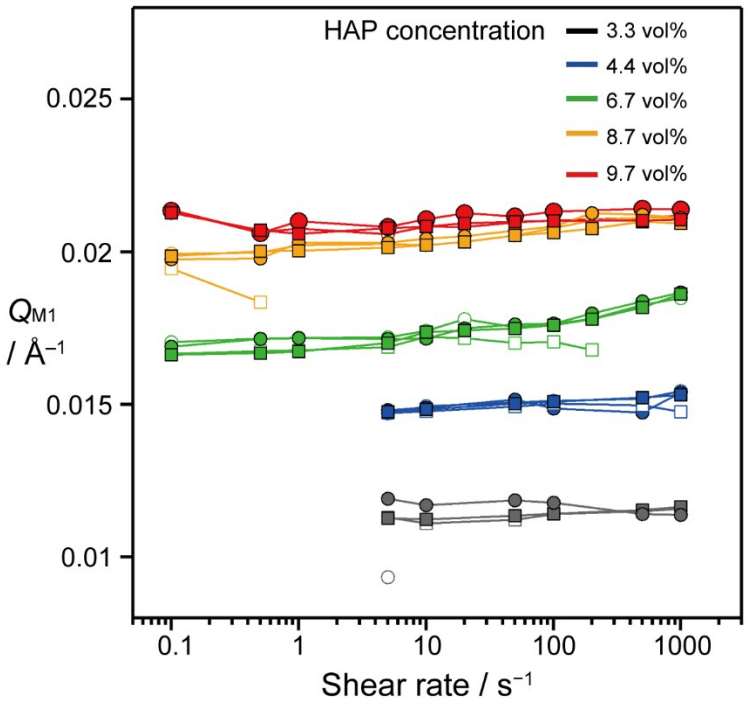

Fig. S18 Peak position Q_{M1} values in SANS profiles for colloidal solutions of HAP-based nanocomposites under shearing force. □: Q_x radial, ■:Q_y radial, ○: Q_x tangential, and ●: Q_y tangential.

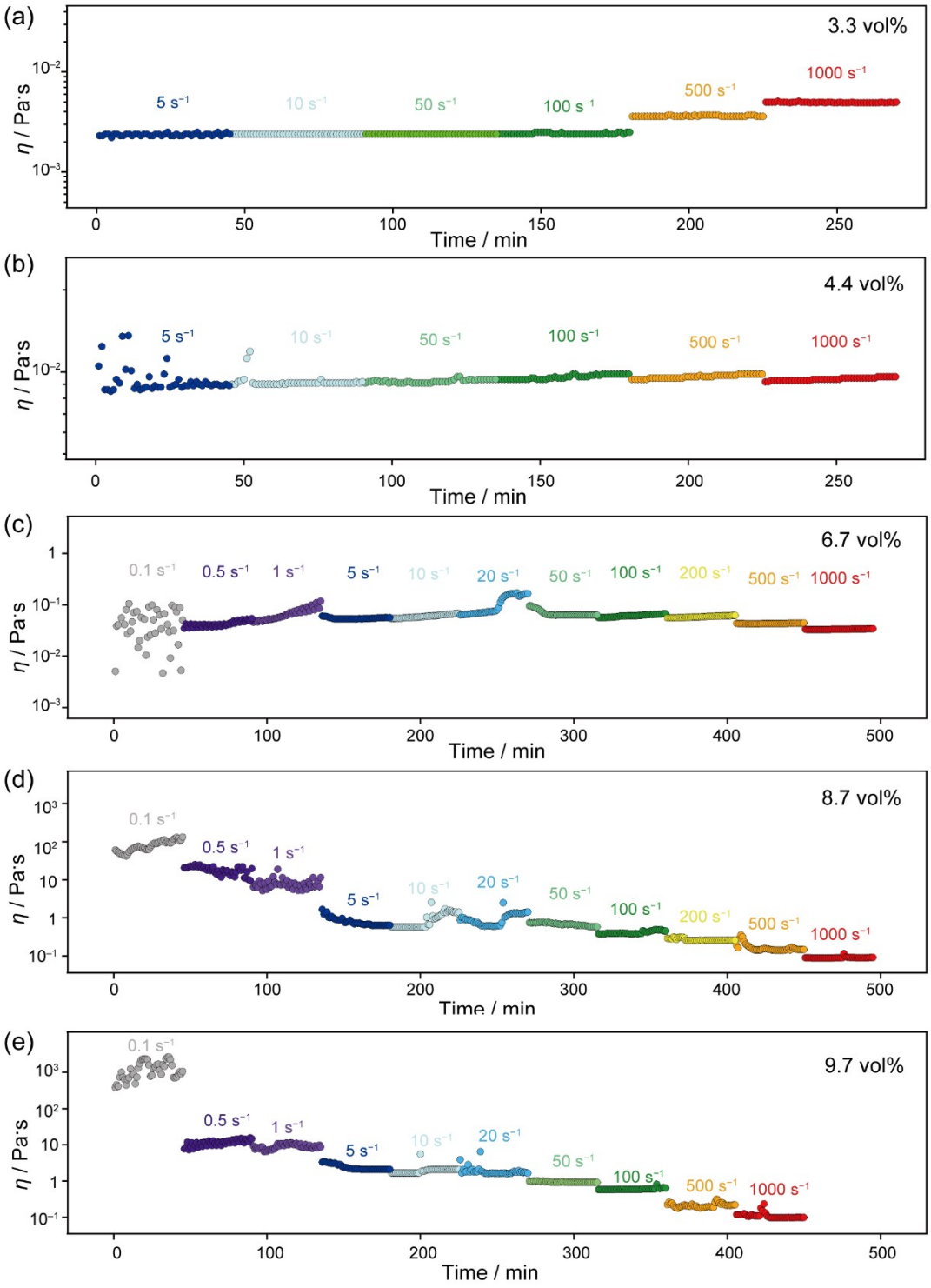

Fig. S19 Viscosity plots under shearing forces of colloidal solutions of HAP-based nanocomposites with various concentrations; (a) 3.3, (b) 4.4, (c) 6.7, (d) 8.7, and (e) 9.7 vol%.

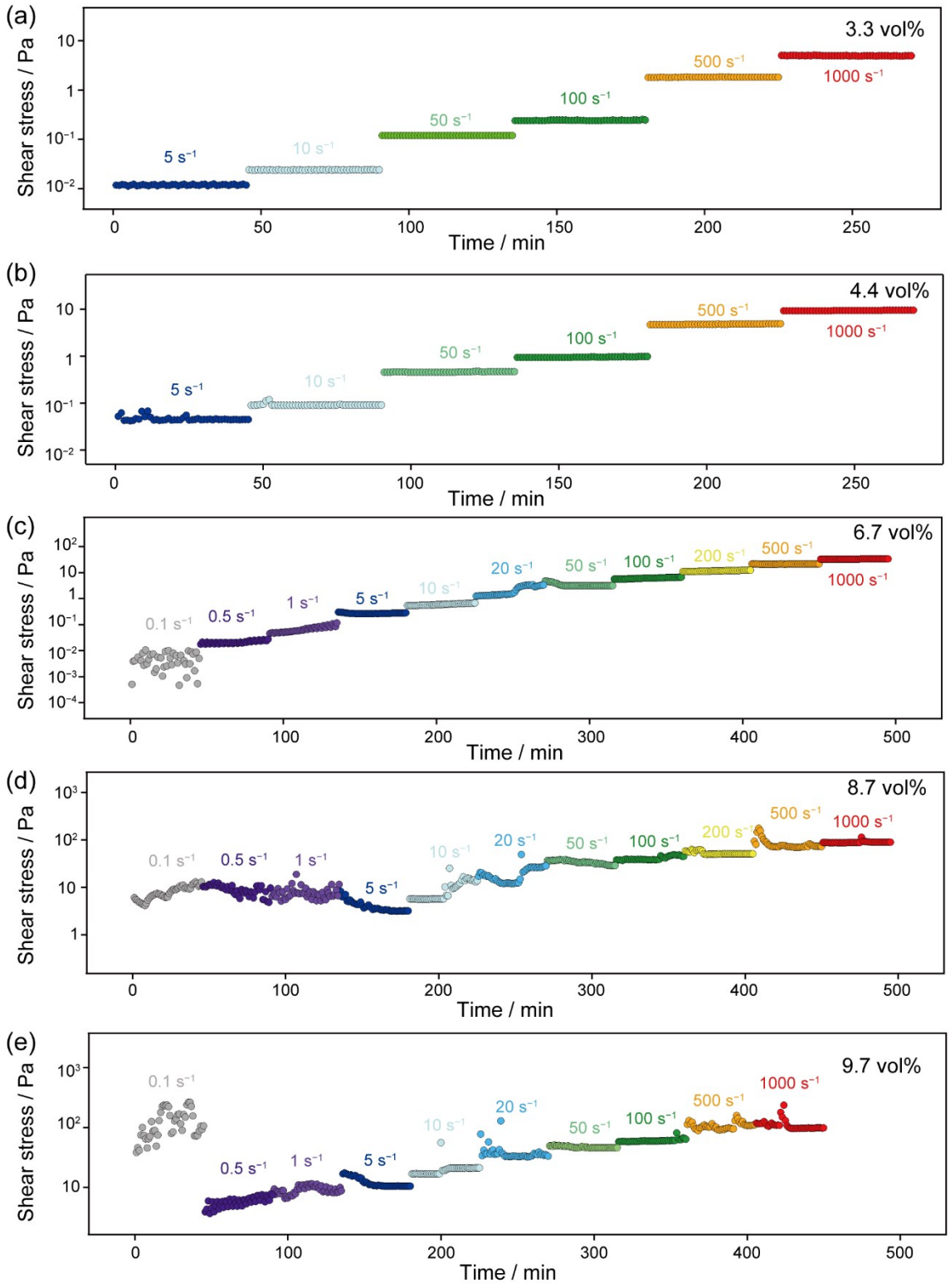

Fig. S20 Shear stress plots under shearing forces of colloidal solutions of HAP-based nanocomposites with various concentrations; (a) 3.3, (b) 4.4, (c) 6.7, (d) 8.7, and (e) 9.7 vol%.